

## Novel Vehicular Trajectories for Collective Motion from Coupled Oscillator Steering Control\*

Margot Kimura<sup>†</sup> and Jeff Moehlis<sup>†</sup>

**Abstract.** We consider a model for vehicle motion coordination for three vehicles that uses coupled oscillator steering control. Prior work on such models has focused primarily on sinusoidal coupling functions, which typically give behavior in which individual vehicles move either in straight lines or in circles. We show that other, more exotic trajectories are possible when more general coupling functions are considered. Such trajectories are associated with periodic orbits in the steering control subsystem. The proximity of these periodic orbits to heteroclinic bifurcations allows for a detailed characterization of the properties of the vehicular trajectories.

**Key words.** collective motion, coupled oscillators

**AMS subject classifications.** 34C15, 93C15, 37C27, 37C29

**DOI.** 10.1137/070704496

**1. Introduction.** Many organisms display ordered collective motion [7], such as geese flying in a Chevron-shaped formation [22], wildebeests herding on the Serengeti plains of Africa [32], locusts swarming in sub-Saharan Africa [34], and fish schooling [28]. Collective motion is also of great interest and importance for engineering applications such as formation control of unmanned vehicles and spacecraft [18, 29, 31], cooperative robotics [8], and sensor networks [9]. Much recent work in the engineering community involves formulating and studying interaction rules which allow a population to operate in a particular collective motion state; e.g., [10, 14, 17, 18, 21, 24, 31].

In the present paper, we consider the “LPS model” for vehicle motion coordination developed by Leonard, Paley, and Sepulchre [25, 26, 27, 29, 30, 31]; cf. [19]. This considers  $N$  Dubins-type vehicles [11] which are identical, move with constant unit speed, and are globally (all-to-all) coupled:

$$(1.1) \quad \begin{aligned} \dot{r}_n &= e^{i\theta_n}, \\ \dot{\theta}_n &= u_n(r, \theta), \quad n = 1, \dots, N. \end{aligned}$$

Here the complex vector  $r_n$  denotes the position of vehicle  $n$  with respect to the origin, while the angle  $\theta_n$  denotes the orientation of its (unit) velocity vector with respect to the positive real axis. Since  $r_n = x_n + iy_n$ , with  $(x_n, y_n) \in \mathbb{R}^2$ , we will hereafter use the following equivalent

---

\*Received by the editors October 4, 2007; accepted for publication (in revised form) by R. Murray July 9, 2008; published electronically October 24, 2008. This work was supported by National Science Foundation grants NSF-0547606 and NSF-0434328 and an Alfred P. Sloan Research Fellowship in Mathematics.

<http://www.siam.org/journals/siads/7-4/70449.html>

<sup>†</sup>Department of Mechanical Engineering, University of California, Santa Barbara, CA 93106 (kimura@engineering.ucsb.edu, moehlis@engineering.ucsb.edu).

equations for the velocity of each vehicle:

$$(1.2) \quad \begin{aligned} \dot{x}_n &= \cos(\theta_n), \\ \dot{y}_n &= \sin(\theta_n). \end{aligned}$$

It can be shown that the system in (1.1) is invariant to rigid group rotation and translation for controllers  $u_n(r, \theta)$  that are functions of only the relative positions and headings of the vehicles, defined as  $r_m - r_n$  and  $\theta_m - \theta_n$ , respectively [25, 26, 27, 29, 30, 31]; cf. [19].

The steering control  $u_n(r, \theta)$  of the vehicles can be decomposed as

$$(1.3) \quad u_n(r, \theta) = \underbrace{\omega_0 + u_n^{head}(\theta)}_{u_n^{phase}(\theta)} + u_n^{spac}(r, \theta), \quad n = 1, \dots, N,$$

where  $\omega_0 \in \mathbb{R}$  is a constant, the heading controller  $u_n^{head}$  depends only on the relative orientation of the vehicles and governs the relative directions, and the spacing controller  $u_n^{spac}$  is used to attract the vehicles to a given spatial formation. Following [27, 29, 31], we call  $u_n^{phase}(\theta)$  the *phase controller*. When the phase controller depends only on the differences  $\theta_m - \theta_n$ , a useful connection with the coupled oscillator literature (e.g., [5, 6, 33]) is possible.

Constructing the spacing controller is more challenging in general, since it must be designed to stabilize a specific formation. In [26, 27, 29, 30, 31], a controller that stabilizes a circular formation and a proof of stabilization are given. The basic idea is to design a potential function which is minimized when the vehicles are in the desired configuration. Then, for  $u_n^{head} = 0$ , it is possible to construct a Lyapunov function to demonstrate that the desired formation is asymptotically stable. For the overall system, one can use a composite Lyapunov function, made up of a linear combination of the Lyapunov functions used for the spacing and heading controls, to prove the stability of the overall desired configuration [25, 26, 27, 29, 30, 31].

The benefits of this type of model for controlling the motion of a group of vehicles are clear: the model takes advantage of results from research on coupled oscillators and translates them into a simple but robust law governing individual vehicle motion that produces the desired overall group motion.

Most of the previous work on the LPS model has assumed a sinusoidal coupling function for the phase controller:

$$(1.4) \quad u_n^{phase} = \omega_0 + \frac{k}{N} \sum_{j=1}^N \sin(\theta_m - \theta_n).$$

With this phase controller alone (i.e.,  $u_n^{spac} = 0$ ), the system converges asymptotically to a synchronized phase arrangement for  $k > 0$ , and a phase-balanced solution for  $k < 0$  [23, 25, 27, 29]. Both of these phase-space solutions lead to vehicular trajectories that are either straight lines or circles, depending on the value of  $\omega_0$ : for  $\omega_0 \neq 0$ , the trajectories converge to circles, and for  $\omega_0 = 0$ , the trajectories converge to straight lines.

In this paper, we explore the effects of more general coupling functions to see what other types of coordinated motion are possible for this model using the phase controller alone. We

will show that one can get trajectories that are much more exotic than straight lines or circles, and which may be advantageous in situations where one wants a relatively complicated trajectory that is a natural result of the phase controller, rather than having to piece a similar trajectory together with existing methods. The trajectories from our phase controller are characterized by almost regular, Spirograph-like shapes, where the vehicles spend some time circling one section of space before moving on to another area, eventually tracing out an annulus, which may be useful in applications where one wants a robot to patrol an appropriately shaped space while periodically doing a more careful search of a subsection of that space. These trajectories are related to heteroclinic cycles for the coupled oscillator system; see [3, 16] for related heteroclinic orbits in systems of  $N$  coupled identical oscillators; cf. [4, 5]. To simplify our analysis, we will restrict the system to three vehicles. (A discussion of more general coupling functions for two vehicles is given in [20].)

We begin with an analysis of the general phase control and then present a detailed analysis of the resulting trajectories for a specific coupling function. Sections 2 and 3 consider the case of all-to-all coupling, while section 4 considers a different coupling topology. Our conclusion is given in section 5.

## 2. Identical all-to-all coupling: Phase dynamics.

**2.1. Equations and symmetry.** A system of three identical oscillators with all-to-all identical phase-difference coupling is given by

$$(2.1) \quad \dot{\theta}_n = \omega_0 + k \sum_{m \neq n} f(\theta_m - \theta_n), \quad n = 1, 2, 3,$$

where  $\theta_n \in [0, 2\pi)$  and the coupling function  $f$  is  $2\pi$ -periodic. This system of equations is equivariant with respect to the group  $S_3 \times T^1$ , where  $S_3$  is the six-element permutation group generated by

$$(2.2) \quad \begin{aligned} \sigma_1 &: (\theta_1, \theta_2, \theta_3) \rightarrow (\theta_2, \theta_1, \theta_3), \\ \sigma_2 &: (\theta_1, \theta_2, \theta_3) \rightarrow (\theta_2, \theta_3, \theta_1), \end{aligned}$$

and  $T^1$  is the circle group with action

$$(2.3) \quad \tau_\phi : (\theta_1, \theta_2, \theta_3) \rightarrow (\theta_1 + \phi, \theta_2 + \phi, \theta_3 + \phi)$$

for all  $\phi \in [0, 2\pi)$ . This means that if  $(\theta_1(t), \theta_2(t), \theta_3(t))$  is a solution to (2.1), then, for any  $\gamma \in S_3 \times T^1$ , so is  $\gamma \cdot (\theta_1(t), \theta_2(t), \theta_3(t))$ .

Equation (2.1) can be reduced to a two-dimensional system by introducing the  $2\pi$ -periodic variables  $\psi_1 = \theta_1 - \theta_2$  and  $\psi_2 = \theta_1 - \theta_3$ :

$$(2.4) \quad \begin{aligned} \dot{\psi}_1 &= \dot{\theta}_1 - \dot{\theta}_2 = k[f(-\psi_1) + f(-\psi_2) - f(\psi_1) - f(\psi_1 - \psi_2)], \\ \dot{\psi}_2 &= \dot{\theta}_1 - \dot{\theta}_3 = k[f(-\psi_1) + f(-\psi_2) - f(\psi_2) - f(\psi_2 - \psi_1)]. \end{aligned}$$

Equation (2.4) inherits equivariance with respect to the actions obtained from (2.2) and (2.3) on the  $\psi$  variables:

$$(2.5) \quad \begin{aligned} \hat{\sigma}_1 &: (\psi_1, \psi_2) \rightarrow (-\psi_1, \psi_2 - \psi_1), \\ \hat{\sigma}_2 &: (\psi_1, \psi_2) \rightarrow (\psi_2 - \psi_1, -\psi_1). \end{aligned}$$

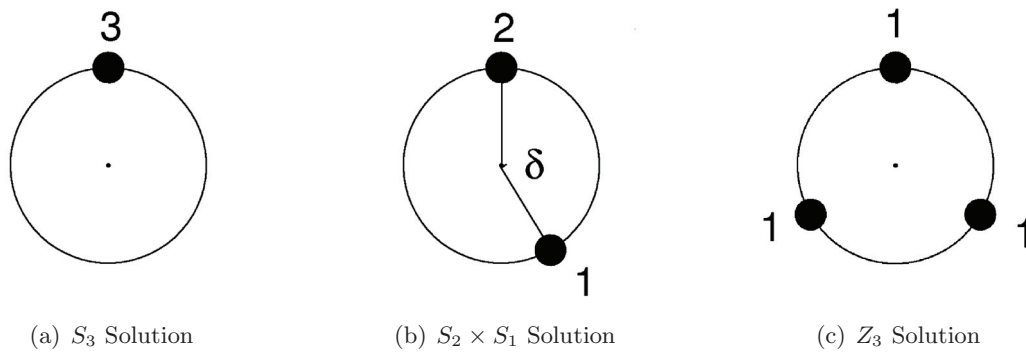


**Figure 1.** Phase-locked solutions guaranteed to exist for any coupling function  $f$ . The locations of the dots on the phase circle are determined by the values of  $\theta$  for the oscillators, with the number indicating how many oscillators share the same phase. These solutions are labeled according to their isotropy subgroup, as described in the text.

Note that  $\hat{\tau}_\phi : (\psi_1, \psi_2) \rightarrow (\psi_1, \psi_2)$  acts as the identity for all  $\phi$ . The actions  $\hat{\sigma}_1$  and  $\hat{\sigma}_2$  generate the permutation group  $S_3$ . We will sometimes find it convenient to think of  $\psi_1$  and  $\psi_2$  as being restricted to  $[0, 2\pi)$ , and other times it will be useful to allow them to take any real value.

**2.2. Solutions and bifurcations.** Phase-locked solutions are characterized by each pair of  $\theta$  variables always differing by a fixed value. Thus in the  $\psi$  variables, phase-locked solutions correspond to fixed points. The symmetry and stability properties of phase-locked solutions are discussed below. As convenient, we will discuss these solutions in either the  $\theta$  or the  $\psi$  variables. The three types of phase-locked solutions shown in Figure 1 are guaranteed to exist for any coupling function  $f$  of the form of (2.1), given a simple nondegeneracy condition [4, 5, 6]. These are labeled according to their isotropy subgroup, which is the set of elements of  $S_3 \times T^1$  that leave the solution unchanged [15]. We note that the existence of a fixed point at  $(\psi_1^*, \psi_2^*)$  implies the existence of fixed points at  $(\psi_1^* + 2\pi j, \psi_2^* + 2\pi m)$  for all  $j \in \mathbb{Z}$  and  $m \in \mathbb{Z}$ .

*The  $S_3$  solutions: Fixed points at  $(\psi_1^*, \psi_2^*) = (0, 0)$ .*

*Symmetry.* This phase-locked solution is invariant under the symmetry  $S_3 = \langle \sigma_1, \sigma_2 \rangle$  in the  $\theta$  variables, and  $S_3 = \langle \hat{\sigma}_1, \hat{\sigma}_2 \rangle$  in the  $\psi$  variables; hence it has the name “ $S_3$  solution.” Since it corresponds to  $\theta_1 = \theta_2 = \theta_3$ , it is also sometimes referred to as the “in-phase” or “synchronous” solution.

*Stability analysis and bifurcations.* The Jacobian for (2.4) at the fixed point  $(\psi_1^*, \psi_2^*) = (0, 0)$  has a double eigenvalue  $\lambda_{1,2} = -3kf'(0)$ . Thus, the stability of the fixed point depends solely on the sign of the real part of  $kf'(0)$ : if  $kf'(0)$  is positive (resp., negative), then the  $S_3$  solution is stable (resp., unstable).

Suppose that there is a bifurcation parameter which causes the shape of the coupling function  $f$  to change. It is immediately evident that the stability of the  $S_3$  fixed point changes if the value  $kf'(0)$  passes through zero as this parameter is varied. Because the fixed point at  $(\psi_1^*, \psi_2^*) = (0, 0)$  will persist for all  $f$ , this corresponds to an  $S_3$ -symmetric transcritical

bifurcation. Assuming that there are no fixed points on the invariant lines  $\psi_1 = 0$ ,  $\psi_2 = 0$ , or  $\psi_1 = \psi_2$ , for  $(\psi_1, \psi_2) \in [0, 2\pi)$ , at this bifurcation, a triangular heteroclinic connection appears between the fixed points at  $(\psi_1^*, \psi_2^*) = (0, 0)$ ,  $(2\pi, 0)$ , and  $(0, 2\pi)$ . Since these points are identified by the  $2\pi$ -periodicity of  $\psi_1$  and  $\psi_2$ , this can also be referred to as a homoclinic connection. Thus, the authors of [4] call this an  $\mathbb{S}_3$  transcritical/homoclinic bifurcation, or  $\mathbb{S}_{3\text{THB}}$ . If the heteroclinic loop is attracting at the bifurcation, the system will have a stable limit cycle very close to the triangle on the side of the bifurcation where the  $S_3$  solution is unstable. Such a bifurcation will occur in the example below.

*The  $S_2 \times S_1$  solutions: Fixed points at  $(\psi_1^*, \psi_2^*) = (0, 2\pi - \delta)$ ,  $(2\pi - \delta, 0)$ , and  $(\delta, \delta)$  for  $\delta \in (0, 2\pi)$ .*

*Symmetry.* Arguments in [5, 6] imply that, provided  $f'(0) \neq 0$ , there must exist a  $\delta \in (0, 2\pi)$  such that there is a phase-locked solution with two oscillators in phase and one oscillator shifted by the phase  $\delta$ . The phase-locked solution corresponding to  $(\psi_1^*, \psi_2^*) = (0, 2\pi - \delta)$  is invariant under the group  $S_2 = \langle \sigma_1 \rangle$  in the  $\theta$  variables, and  $S_2 = \langle \hat{\sigma}_1 \rangle$  in the  $\psi$  variables. Following [5], this is referred to as an  $S_2 \times S_1$  solution: the  $S_2$  corresponds to the permutation just mentioned, and the  $S_1$  refers to the identity permutation acting on the other oscillator. The other phase-locked solutions are related to this one by symmetry and are invariant under conjugate subgroups.

*Stability analysis and bifurcations.* The Jacobian at the fixed point  $(2\pi - \delta, 0)$  has eigenvalues  $\lambda_1 = k[-f'(\delta) - 2f'(-\delta)]$  and  $\lambda_2 = k[-2f'(0) - f'(\delta)]$ . Note that the symmetry-related fixed points at  $(2\pi - \delta, 0)$  and  $(\delta, \delta)$  have the same stability. These points can be sinks, sources, or saddles.

Bifurcations occur when either  $f'(\delta) + 2f'(-\delta) = 0$  or  $f'(\delta) + 2f'(0) = 0$ . Depending on the relative values of  $f'(\delta)$ ,  $f'(-\delta)$ , and  $f'(0)$  for different parameters of  $f$ , the fixed points' stability can change to or from a sink, source, or saddle in a pitchfork or saddle-node bifurcation; cf. [4]. Such solutions are involved in the  $\mathbb{S}_{3\text{THB}}$  bifurcation described above, and can also be involved in the related global saddle-node heteroclinic bifurcation identified in [2].

*The  $Z_3$  solutions: Fixed points at  $(\psi_1^*, \psi_2^*) = (\frac{2\pi}{3}, \frac{4\pi}{3})$  and  $(\frac{4\pi}{3}, \frac{2\pi}{3})$ .*

*Symmetry.* The fixed point  $(\psi_1^*, \psi_2^*) = (\frac{2\pi}{3}, \frac{4\pi}{3})$  corresponds to a solution for which  $\theta_1 = \theta_2 + \frac{2\pi}{3}$  and  $\theta_2 = \theta_3 + \frac{2\pi}{3}$ . This is typically called the “splay state” because  $\theta_1$ ,  $\theta_2$ , and  $\theta_3$  are equally spaced around the unit circle. This solution is invariant under the three-element cyclic group  $Z_3$  generated by

$$(2.6) \quad (\theta_1, \theta_2, \theta_3) \rightarrow \left( \theta_2 + \frac{2\pi}{3}, \theta_3 + \frac{2\pi}{3}, \theta_1 + \frac{2\pi}{3} \right)$$

and hence is called the “ $Z_3$  solution.” In terms of the  $\psi$  variables, this solution is invariant under  $\langle \hat{\sigma}_2 \rangle$ , which is isomorphic to the group  $Z_3$ . The fixed point  $(\psi_1^*, \psi_2^*) = (\frac{4\pi}{3}, \frac{2\pi}{3})$  is invariant under the group  $Z_3$  generated by

$$(2.7) \quad (\theta_1, \theta_2, \theta_3) \rightarrow \left( \theta_3 + \frac{2\pi}{3}, \theta_1 + \frac{2\pi}{3}, \theta_2 + \frac{2\pi}{3} \right)$$

in the  $\theta$  variables and  $\langle \hat{\sigma}_2 \hat{\sigma}_1 \rangle$  in the  $\psi$  variables.

*Stability analysis and bifurcations.* The Jacobian at this fixed point  $(\frac{2\pi}{3}, \frac{4\pi}{3})$  has eigenvalues  $\lambda_{1,2} = k[-\frac{3}{2}(f'(\frac{2\pi}{3}) + f'(\frac{4\pi}{3})) \pm \frac{3i}{2}|f'(\frac{4\pi}{3}) - f'(\frac{2\pi}{3})|]$ . Thus, unless  $f'(\frac{4\pi}{3}) = f'(\frac{2\pi}{3})$ ,

this fixed point will be either a spiral sink or a spiral source. At  $f'(\frac{2\pi}{3}) + f'(\frac{4\pi}{3}) = 0$ , the fixed point switches between a spiral sink and a spiral source, which is an indication of a Hopf bifurcation, as found in [4].

**2.3. An example.** As an example, we now consider the coupling function

$$(2.8) \quad f(\varphi) = \mu_1 \sin(\varphi) + \mu_2 \cos(\varphi) + \mu_3 \sin(2\varphi),$$

which will provide a spectrum of novel trajectories when applied to vehicle motion coordination using the LPS model. While the coupling function given by (2.8) provides a nice example for our analysis of these interesting trajectories, the phenomena that produce the trajectories we consider are fairly generic, and so we expect to see similar bifurcations in the phase space and trajectories for the vehicles for other appropriate coupling functions [3, 16].

The above analysis predicts that both a  $\mathbb{S}_{3\text{THB}}$  bifurcation involving the  $S_3$  and  $S_2 \times S_1$  solutions and, independently, a Hopf bifurcation involving the  $Z_3$  solutions will occur at  $\mu_1 + 2\mu_3 = 0$  for the system (1.1) with coupling function (2.8). Numerical bifurcation analysis using XPPAUT [12] shows that for  $\mu_2 = 1$ ,  $\mu_3 = -0.06$ , and  $k = 1$  and when treating  $\mu_1$  as the bifurcation parameter, the Hopf bifurcation is subcritical, and that the branch of unstable periodic orbits turns around in a saddle-node bifurcation of periodic orbits to give stable periodic orbits; see Figure 2. This figure also illustrates that the phase space for the system can be divided into two triangles bounded by the invariant lines  $\psi_1 = 0$ ,  $\psi_1 = 2\pi$ ,  $\psi_2 = 0$ ,  $\psi_2 = 2\pi$ , and  $\psi_1 = \psi_2$ . Trajectories in these triangles are related by symmetry, and the resulting vehicular trajectories are identical. Thus, without loss of generality, we will assume that all initial conditions are chosen such that the system moves in the lower right triangle.

**3. Identical all-to-all coupling: Vehicular trajectories.** We now illustrate the richness of possible vehicular trajectories for (1.1) with identical all-to-all phase-difference steering control by considering the coupling function given in (2.8) with parameters  $\mu_1 = 0.1$ ,  $\mu_2 = 1$ , and  $\mu_3 = -0.06$ ; see Figure 2(c) for the corresponding reduced phase-space system. If the system converges to the stable  $Z_3$  solution, then the vehicles will move either in circles or in straight lines, depending on the value of  $\omega_0$ , with each instantaneously moving in a direction at an angle of  $\pm \frac{2\pi}{3}$  with respect to the others. Such motion has been found for the LPS model with the coupling function  $f(\theta) = \sin(\theta)$  [25, 26, 27, 29, 30, 31]. However, if the system converges to the stable limit cycle, then the vehicles can display more exotic trajectories, such as the trajectory shown in Figure 3. Thus, we will focus our analysis on the solutions that converge to the stable limit cycle. As we will demonstrate later, these exotic trajectories are products of a stable limit cycle in the reduced phase system, so one can expect to see qualitatively similar trajectories for other appropriate coupling functions and coupling topologies.

Motion along the limit cycle is not uniform: the system slows near each of the fixed points and moves quickly in regions away from a fixed point. As will be explained in the following, it is from this nonuniform motion that the trajectories get their peculiar shapes. We first present an explanation of the vehicular motion in an intuitive way, and then validate the intuition with results from numerical simulations, which were done using a fourth-order variable-timestep Runge–Kutta algorithm. Without loss of generality, we will restrict discussion to the motion of vehicle 1 (denoted  $v_1$ ) only. The motion of vehicle 2 ( $v_2$ ) and vehicle 3 ( $v_3$ ) is identical to but out of phase with the motion of  $v_1$ ; this is summarized in Table 1.

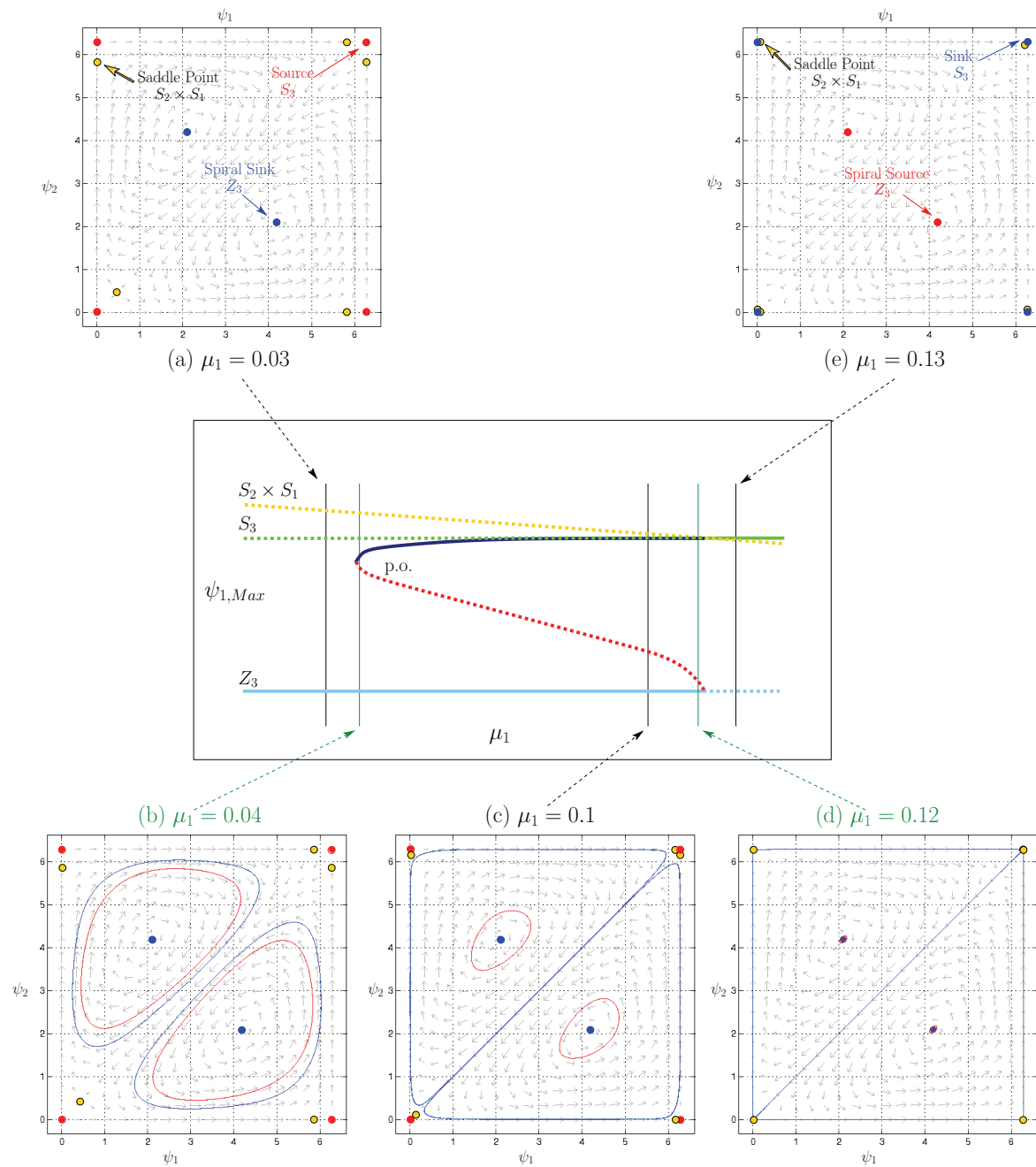


**Figure 2.** The bifurcation diagram in terms of  $\mu_1$ , showing the phase portraits at several values of  $\mu_1$  of interest for  $\mu_2 = 1$  and  $\mu_3 = -0.06$ . In the  $(\psi_1, \psi_2)$  plane, yellow dots represent saddle points, red shows sources or unstable periodic orbits, and blue represents sinks or stable periodic orbits. Solid (resp., dashed) lines in the bifurcation diagram indicate stable (resp., unstable) solutions.

**3.1. The intuitive description.** The overall vehicle motion in Figure 3 can be decomposed into identical units, each of which contains a cluster and a tail. We will name the tail

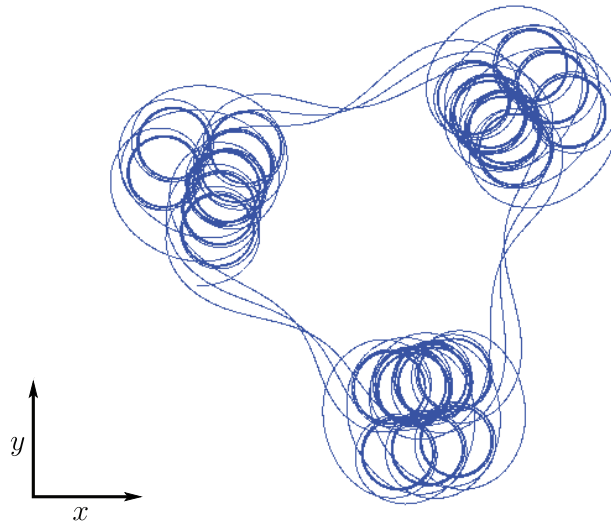


**Figure 3.** An example trajectory for vehicle 1 ( $v_1$ ) with parameters  $\mu_1 = 0.1$ ,  $\mu_2 = 1$ ,  $\mu_3 = -0.06$ ,  $\omega_0 = k = 1$ . This trajectory is taken over many cycles of the periodic orbit in the  $(\psi_1, \psi_2)$  plane.

**Table 1**

Relative phase and resulting behavior of all three vehicles in terms of position in the  $(\psi_1, \psi_2)$  plane. Here,  $\uparrow$  means “increase(s),” and  $\downarrow$  means “decrease(s).” The definition of “excursion” is given in the text.

| Box | $\psi$ behavior   | $\theta$ behavior  | Vehicle motion  |
|-----|---|--|---|
| 1   | $\psi_1 \uparrow$ to $\approx 2\pi$<br>$\psi_2 \approx 0$     | $\theta_1$ & $\theta_3 \uparrow$ at the same rate<br>$\theta_2$ temporarily $\downarrow$ | $v_1$ & $v_3$ : short excursion<br>$v_2$ : long excursion |
| 2   | $\psi_2 \uparrow$ to $\approx 2\pi$<br>$\psi_1 \approx 2\pi$  | $\theta_1$ & $\theta_2 \uparrow$ at the same rate<br>$\theta_3$ temporarily $\downarrow$ | $v_1$ & $v_2$ : short excursion<br>$v_3$ : long excursion |
| 3   | $\psi_1 \approx \psi_2 \downarrow$<br>together to $\approx 0$ | $\theta_2$ & $\theta_3 \uparrow$ at the same rate<br>$\theta_1$ temporarily $\downarrow$ | $v_2$ & $v_3$ : short excursion<br>$v_1$ : long excursion |

connecting the units a *long excursion*. Each cluster can be further broken down to show two general types of behavior: small approximately circular orbits, which we will call *small orbits*, and the roughly semicircular excursions that connect the small orbits, which we will refer to as *short excursions*. The vehicle path in a single unit can be described as a cycle through a small orbit followed by a short excursion to another small orbit, followed by a second short excursion to a third small orbit, followed by a long excursion to the next cluster. This is illustrated in Figure 4.

We can understand this behavior by dividing the periodic orbit into six boxes, as labeled in Figure 4. Simulations show that when the system in the  $(\psi_1, \psi_2)$  plane is in a lettered box (i.e., near a fixed point), the vehicles move in a small orbit, and when the system is in a numbered box, the vehicles undergo an excursion. This is expected, since the vehicles would move in a circle if the system were actually at the fixed point (i.e., generically, at a fixed point,  $\dot{\theta}_j = \text{constant} \neq 0$ ). Therefore, one can intuitively expect the vehicles to show switching behavior between small orbits and excursions as the system moves in the  $(\psi_1, \psi_2)$  plane.

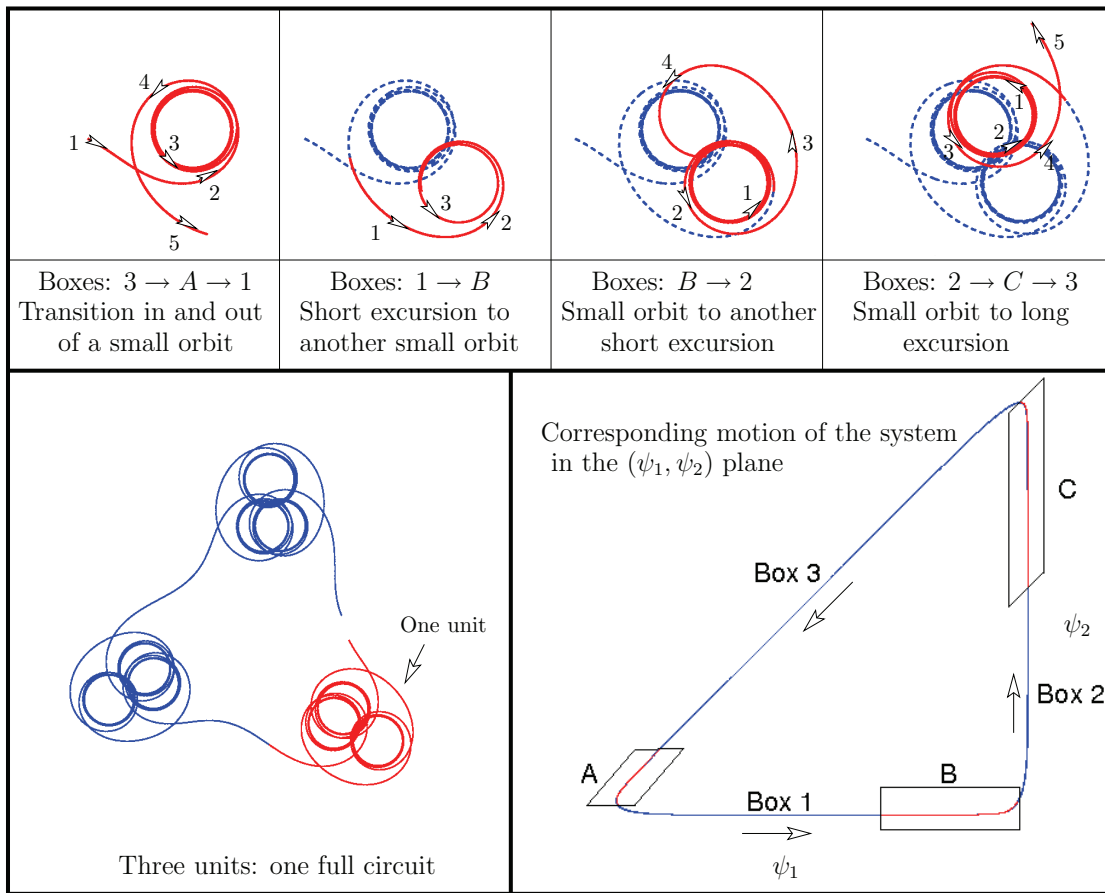


**Figure 4.** Behavior of  $v_1$  in the  $(x, y)$  plane with corresponding position of the system in the  $(\psi_1, \psi_2)$  plane. The top explains the motion of  $v_1$  within one unit: Follow the ordered arrows in the time-series of pictures. The bottom-left panel shows one full circuit of vehicle motion, and the bottom-right panel shows the various boxes in the  $(\psi_1, \psi_2)$  plane.

### 3.2. Numerical analysis and validation.

**3.2.1. Box definition.** To validate the above intuition, we need to be more precise about the boundaries of the boxes. Since the vehicles are always moving in a smooth and roughly circular trajectory, it is natural to define the boxes in terms of the instantaneous radius of curvature of the vehicles' trajectories. This was calculated from simulation data for each point by finding the radius of the circle defined by that point and its two neighboring points; see Figure 5.

The lettered boxes were chosen by calculating where the radius of curvature for  $v_1$  was within 0.01 of the minima of each trough, as seen in Figure 6. Boxes 1, 2, and 3 are then defined as the intervening lengths of the periodic orbit in the  $(\psi_1, \psi_2)$  plane.

**3.2.2. Approximate solutions.** Within each box, we present an approximate solution with a few simplifying assumptions.

Near a fixed point (i.e., in a lettered box), the behavior of the system is approximately

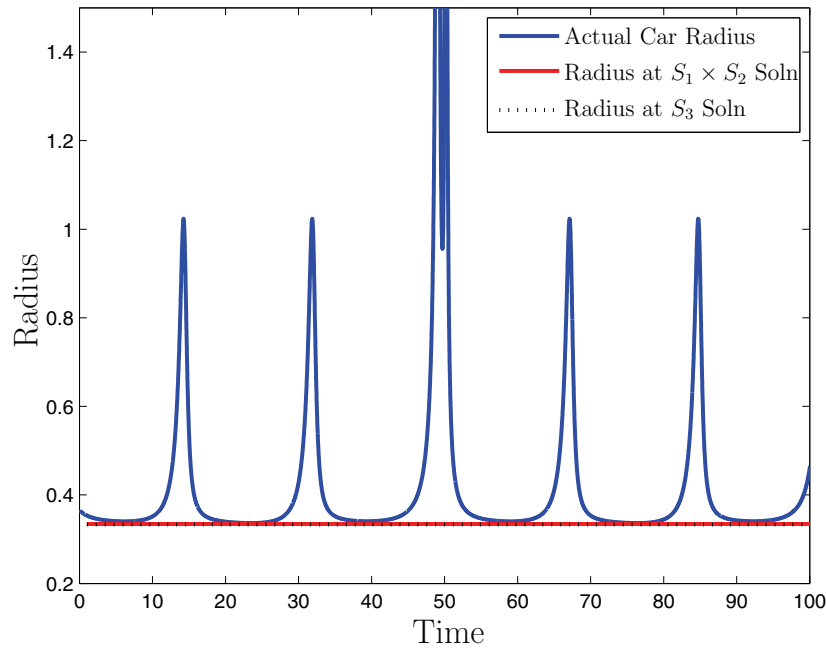


**Figure 5.** Measurements of the radius of curvature for  $v_1$  moving in the trajectory shown in Figure 3 with the approximations at each nearby fixed point. It is evident from the periodic flat troughs that the radius of curvature of the vehicles' motion spends a significant amount of time at an approximately constant value. Moreover, the value of that constant value is very close to the radius of curvature the vehicles' motion would have if the system were at the  $S_2 \times S_1$  solution. See Figure 6 for an enlargement.

the same as if the system were actually at the fixed point. At a fixed point, we have  $\dot{\theta}_1 = \dot{\theta}_2 = \dot{\theta}_3 \equiv \varpi$ , where  $\varpi$  is a constant. This is easily integrated, giving

$$\theta_i(t) = \varpi t + \theta_{0i}.$$

This corresponds to the following equations in the  $(x, y)$  plane:

$$\begin{aligned} \dot{x}_i &= \cos(\varpi t + \theta_{0i}), \\ \dot{y}_i &= \sin(\varpi t + \theta_{0i}). \end{aligned}$$

These equations can also be integrated, yielding

$$\begin{aligned} x_i &= \frac{1}{\varpi} \sin(\varpi t + \theta_{0i}), \\ y_i &= -\frac{1}{\varpi} \cos(\varpi t + \theta_{0i}), \end{aligned}$$

corresponding to motion in a circle of radius  $\frac{1}{\varpi}$ .

For the particular coupling function discussed in the example above,  $\varpi = \omega_0 + 2k\mu_2$ . Plugging in  $\omega_0 = k = \mu_2 = 1$ , we find that the vehicles move in circles with radius  $\frac{1}{3}$  if the system is at an  $S_3$  solution. When the system is at one of the  $S_2 \times S_1$  solutions, found for

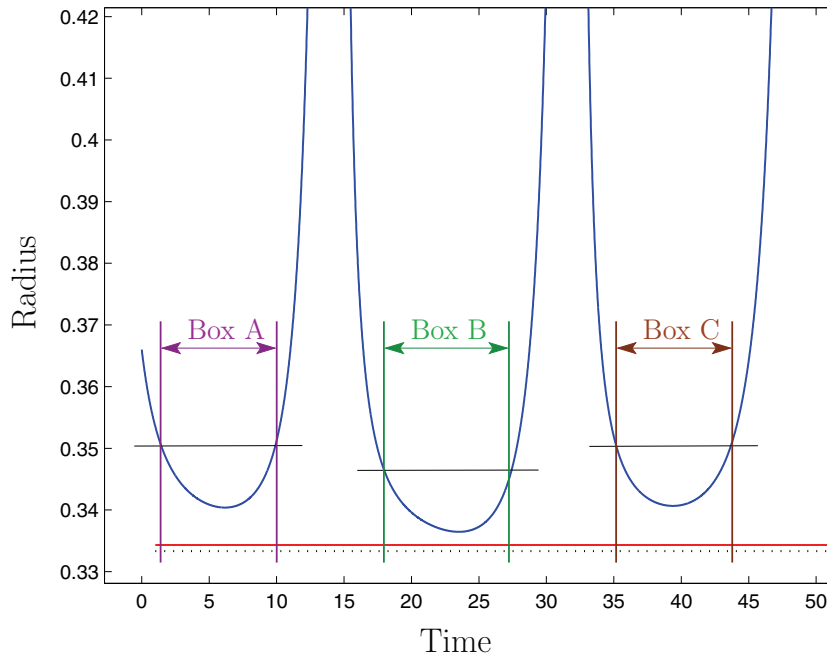


**Figure 6.** An enlargement of Figure 5, showing how close the actual instantaneous radius of curvature of  $v_1$  comes to the approximated values, and how the radius of curvature defines the location of the lettered boxes. The dotted line represents what the radius of curvature would be at the  $S_3$  solution, and the red solid line represents the radius at the  $S_2 \times S_1$  solution. The line segments show where the radius of curvature of  $v_1$  is within 0.01 of its minimum for each box. The edges of the boxes correspond to the intersections of these line segments with the radius of curvature of  $v_1$ . The numbered boxes are then assigned as the intervening spaces between lettered boxes.

these parameters to be at  $(0.11511, 0.11511)$ ,  $(0, 2\pi - 0.11511)$ , or  $(2\pi - 0.11511, 0)$ , the radius of the motion of  $v_1$  is approximately 0.334317. As one can see in Figure 6, the approximation that the system is at an  $S_2 \times S_1$  fixed point is very close to the results obtained from the actual simulation.

In the numbered boxes, we can approximate the behavior of the system by noting that in Box 1,  $\psi_2 \approx 0$ , in Box 2,  $\psi_1 \approx 0$ , and in Box 3,  $\psi_1 \approx \psi_2$  and both decrease from a value close to  $2\pi$  to a value close to 0 at about the same rate.

Taking  $\psi_2 = 0$  (which is approximately true in Box 1) in (2.4), we obtain  $\dot{\psi}_2 = 0$  and

$$(3.1) \quad \dot{\psi}_1 = \dot{\theta}_1 - \dot{\theta}_2 = k[f(-\psi_1) + f(0) - 2f(\psi_1)],$$

a one-dimensional differential equation. Similarly, taking  $\psi_1 = 2\pi = 0$  (which is approximately true in Box 2) in (2.4) gives the same formula as (3.1) but with  $\psi_1 \rightarrow \psi_2$ . Finally, taking  $\psi_1 = \psi_2 \equiv \psi$  (which is approximately true in Box 3), we obtain

$$(3.2) \quad \dot{\psi}_1 = \dot{\psi}_2 = \dot{\psi} = k[2f(-\psi) - f(0) - f(\psi)],$$

which is related to (3.1) through  $\psi_1 \rightarrow -\psi$ .

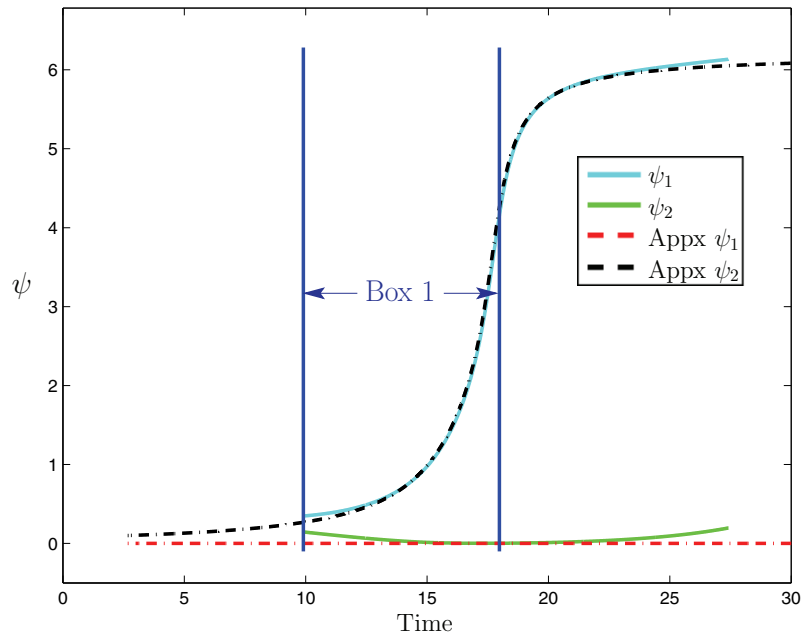


**Figure 7.** Demonstration of the validity of the approximation leading to (3.1): The graphs of the approximate solutions in Box 1 and actual simulation data show that the assumptions made are reasonable.

Numerical integration of the approximate equations very closely matches the data from simulation in all three boxes; see Figures 7 and 8 for Boxes 1 and 3, respectively. (The approximate solutions are nearly identical in Boxes 1 and 2, so only the simulation for Box 1 is shown.)

**3.2.3. The Spirograph kaleidoscope.** The  $\omega_0$  and  $k$  terms effectively control the curvature of the individual trajectories and the speed at which the system moves through the  $(\psi_1, \psi_2)$  plane, respectively. The shape of the vehicular trajectories, even in transients, depends only on the ratio  $\frac{\omega_0}{k}$ , as can be seen most easily in an equivalent form of (2.1):

$$(3.3) \quad \dot{\theta}_n = k \left( \frac{\omega_0}{k} + \sum_{m \neq n} f(\theta_m - \theta_n) \right), \quad n = 1, 2, 3.$$

In this form, it is clear that the variable  $k$  simply scales time, while the actual dynamics depend only on the constant  $\frac{\omega_0}{k}$ , which can be thought of as the effective natural frequency. Since we have constrained our vehicles to have constant unit velocity, the only way that the vehicles can compensate for a larger (resp., smaller)  $k$  (with appropriately scaled  $\omega_0$ ), which would make the vehicles move more quickly (resp., slowly), is to produce a smaller (resp., larger), scaled, version of the exact same pattern, even in transients. This effect is demonstrated in Figure 9.

There are many possible trajectories found by varying the  $\frac{\omega_0}{k}$  ratio, which have a base shape

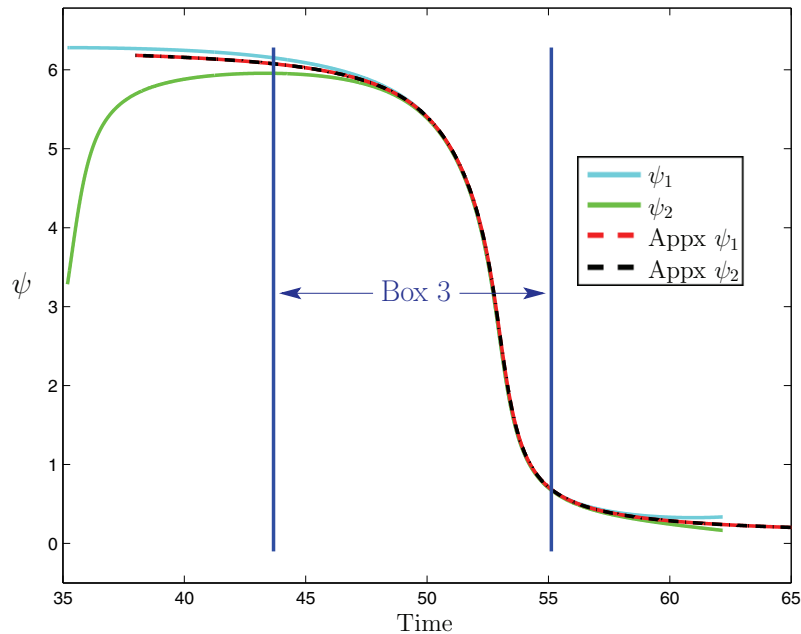


**Figure 8.** Demonstration of the validity of the approximation leading to (3.2): The graphs of the approximate solutions in Box 3 and actual simulation data show that the assumptions made are reasonable.

resembling a pattern from a Spirograph.<sup>1</sup> It is possible to obtain a regular overall trajectory (global) shape with any number of sides that either passes through the approximate center of the polygon, or travels exclusively along the edges. In other words, the radius of the global shape can be made to be anywhere between zero and infinity. Moreover, as one steps through the possible values of  $\frac{\omega_0}{k}$ , the radius runs continuously from zero through infinity and back to zero again, providing a kaleidoscope-like effect. Recognition of this trend allows one to look at a trajectory for a given set of parameters, and to be able to expect roughly what the trajectories will look like for neighboring values of  $\frac{\omega_0}{k}$ .

To sample over the different types of trajectories possible for  $\omega_0 > 0$  and  $k > 0$ , we first held  $\omega_0 = 1$  and varied  $k$  from 0 to 1, and then held  $k = 1$  and varied  $\omega_0$  from 0 to 1. Some example trajectories are shown in Figures 10 and 11. From simulations, we have found that the global radius goes to infinity when  $\frac{\omega_0}{k} \approx 0.1292 + 0.1189n$ , where  $n$  is an integer.

**4. The Arbiter configuration.** We have also found interesting phase dynamics and vehicular trajectories for coupling topologies other than all-to-all. Here we focus on the coupling topology shown in Figure 12, which we have nicknamed the “Arbiter” configuration.

<sup>1</sup>A “Spirograph” is a toy invented by Denys Fisher and was first introduced to the United States in 1966 by Kenner, Inc. The name “Spirograph” is a trademark of Hasbro, Inc. The toy allows the user to create intricate designs: The user puts a pen on a point within a circle, which rotates around the inside or outside of another shape, typically also a circle. The geometric curves produced by a Spirograph are mathematically known as hypotrochoids and epitrochoids [1]. An interactive applet demonstrating what patterns are possible with a Spirograph can be found at [13].

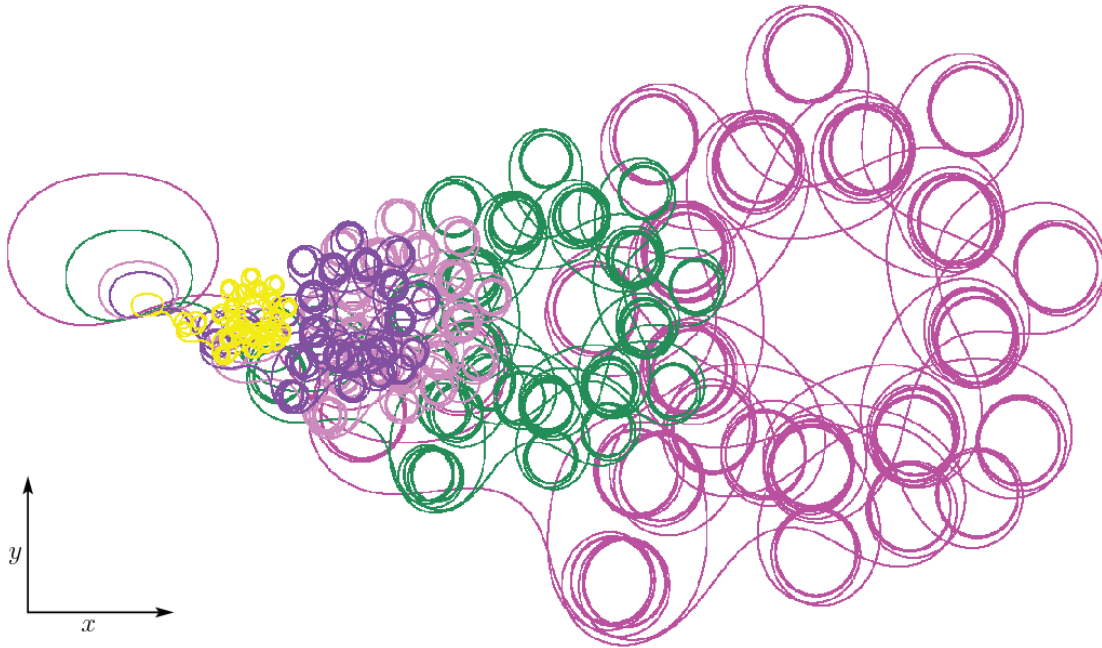


**Figure 9.** Five trajectories with the same initial conditions in  $(x, y)$  and  $(\psi_1, \psi_2)$ , and with the same ratio  $\frac{\omega_0}{k}$ , but with different values of  $k$  (and appropriately scaled  $\omega_0$ ).

The equations for the Arbiter configuration for  $N = 3$  are

$$(4.1) \quad \begin{aligned} \dot{\theta}_1 &= \omega_0 + k[f(\theta_2 - \theta_1) + f(\theta_3 - \theta_1)], \\ \dot{\theta}_2 &= \omega_0 + kf(\theta_1 - \theta_2), \\ \dot{\theta}_3 &= \omega_0 + kf(\theta_1 - \theta_3). \end{aligned}$$

Transforming (4.1) into the  $\psi$  coordinates as in section 2.3 gives

$$(4.2) \quad \begin{aligned} \dot{\psi}_1 &= k[f(-\psi_1) + f(-\psi_2) - f(\psi_1)], \\ \dot{\psi}_2 &= k[f(-\psi_1) + f(-\psi_2) - f(\psi_2)]. \end{aligned}$$

It is evident that the  $(\psi_1, \psi_2)$  equations are equivariant under permutation of  $\psi_1$  and  $\psi_2$ , and that the lines  $\psi_1 = 2\pi n$  and  $\psi_2 = 2\pi n$ , where  $n$  is an integer, are no longer invariant. The system does have an invariant line at  $\psi_1 = \psi_2$ . Along this line,  $\psi_1 = \psi_2 \equiv \psi$ , and we see that if there exists a  $\delta^*$  such that  $2f(-\delta^*) - f(\delta^*) = 0$ , then there will be at least one fixed point on the invariant line at  $(\psi_1, \psi_2) = (\delta^*, \delta^*)$ . An argument for the existence of such a  $\delta^*$  under quite general conditions follows.

**4.1. Existence of  $S_2 \times S_1$  solutions with  $\psi_1 = \psi_2$ .** Letting

$$(4.3) \quad c_1(\delta) = 2f(-\delta), \quad c_2(\delta) = f(\delta),$$

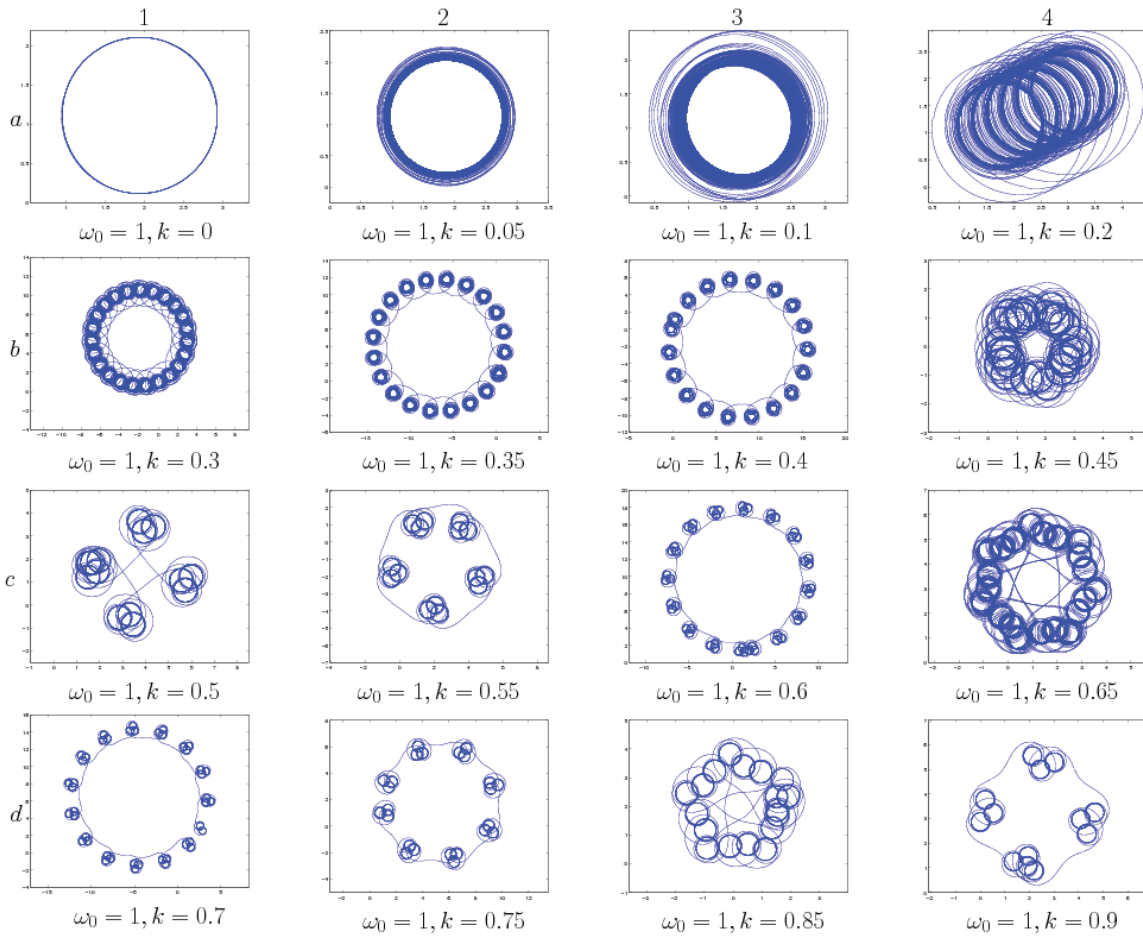


**Figure 10.** A few examples of vehicular trajectories for  $v_1$  from coupling function (2.8) with  $\mu_1 = 0.1$ ,  $\mu_2 = 1$ , and  $\mu_3 = -0.06$ , while holding  $\omega_0 = 1$  and varying  $k$  from 0 to a value close to 1.

a valid  $\delta^*$  will satisfy

$$(4.4) \quad c_1(\delta^*) = c_2(\delta^*).$$

If  $|f(\delta)| \geq 0$  for all  $\delta$ , it is possible that no such  $\delta$  exists: for example, take  $f(\delta) = 1$ . Therefore, we assume that there exists a  $\phi_1 \neq 0$  such that  $f(\phi_1) = 0$ , but  $f'(\phi_1) \neq 0$ . Then, by periodicity of  $f$ , there must be a  $\phi_2 \neq 0$  such that  $f(\phi_2) = 0$  but  $f'(\phi_2) \neq 0$ .

If  $f(0) \neq 0$ , without loss of generality, we can assume that  $c_1(0) > c_2(0) > 0$ . This implies that  $c_1(2\pi) > c_2(2\pi) > 0$ . Now,

$$\begin{aligned} \min[c_2(\delta)] &= \min[f(\delta)] \equiv \beta, \\ \min[c_1(\delta)] &= \min[2f(-\delta)] = \min[2f(\delta)] = 2[\min f(\delta)] = 2\beta, \end{aligned}$$

where  $\beta < 0$ , as shown in Figure 13. This implies that there exists a  $\delta^{**}$  such that  $c_1(\delta^{**}) < c_2(\delta^{**})$ . Therefore, by the intermediate value theorem, there must be at least two valid values

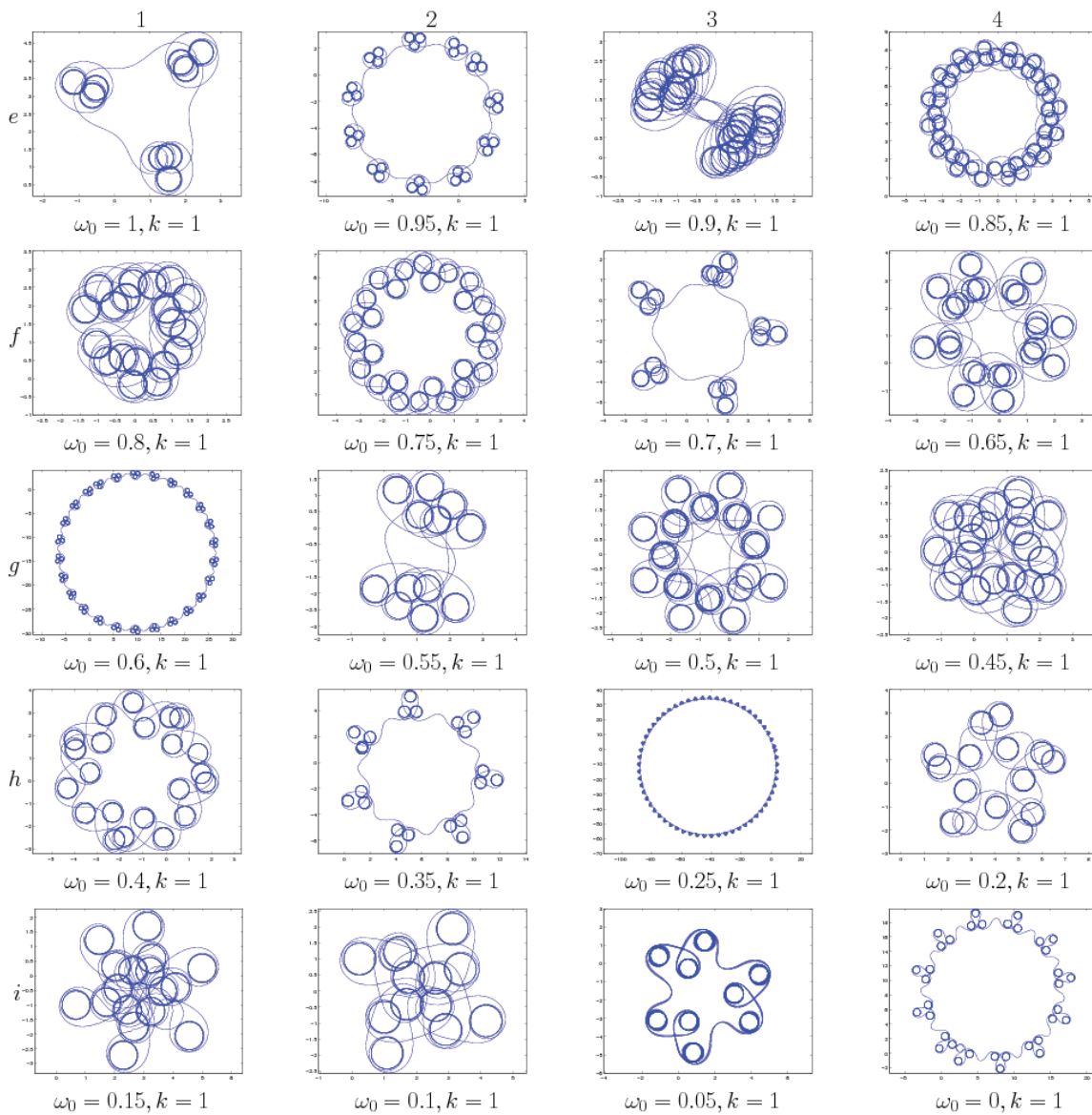


**Figure 11.** A continuation of Figure 10: A few example vehicular trajectories for  $v_1$  holding  $k = 1$  and varying  $\omega_0$  from 1 to 0.

$\delta_{1,2}^*$  such that  $c_1(\delta_1^*) = c_2(\delta_1^*)$  and  $c_1(\delta_2^*) = c_2(\delta_2^*)$ . Furthermore, all further viable values for  $\delta^*$  will occur in pairs.

A similar argument can be made to prove the existence of a  $\delta^* \in (0, 2\pi)$  if  $f(0) = 0$  (corresponding to the existence of an  $S_3$ -symmetric fixed point) provided that there exists a  $\phi_1 \neq 0$  such that  $f(\phi_1) = 0$  and  $f'(\phi_1) \neq 0$ .

**4.2. Example.** Using the example coupling function (2.8) with  $\mu_1 = 0.1$ ,  $\mu_2 = 1$ ,  $\mu_3 = -0.06$ , and  $k = 1$ , we find that the system has saddle points at  $(\psi_1^*, \psi_2^*) = (4.29213, 4.29213)$

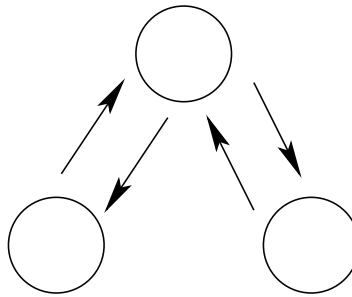


**Figure 12.** The Arbitrator configuration. Here the arrows indicate the coupling between agents.

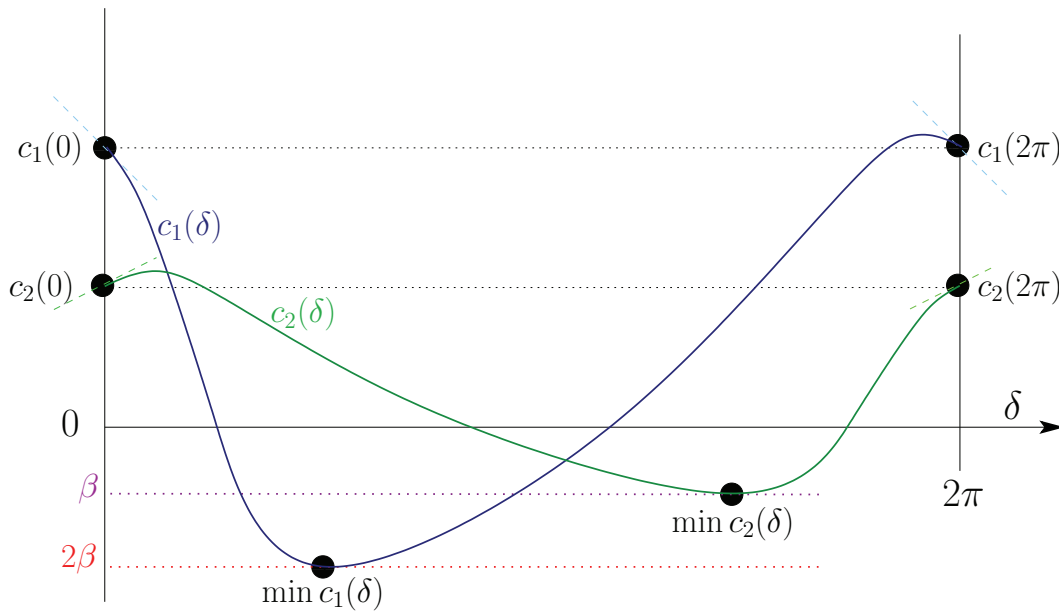


**Figure 13.** Illustration of the argument that given the constraints mentioned in the text, there must be at least two possible values for  $\delta^*$ . Without loss of generality, we can set  $c_1(0) > c_2(0) > 0$ , which gives  $c_1(2\pi) > c_2(2\pi) > 0$  by periodicity. However, by noting that  $\min[f(-\delta)] = \min[f(\delta)]$ , it is clear that  $\min[c_1(\delta)] = 2 \min[c_2(\delta)]$ . Therefore,  $c_1(\delta)$  and  $c_2(\delta)$  must cross in at least two points. The points where the two functions cross are viable values for  $\delta^*$ , and this proves the existence of the  $S_2 \times S_1$  solutions.

and  $(1.35235, 1.35235)$ , which are guaranteed to exist from the above argument, and spiral sinks at  $(\psi_1^*, \psi_2^*) = (4.8432, 1.63105)$  and  $(1.63105, 4.8432)$ . For these parameters, there are also two symmetry-related stable periodic orbits in the  $(\psi_1, \psi_2)$  coordinates; see Figure 14. The vehicular trajectories corresponding to motion along several cycles of one of the stable periodic orbits is shown in Figure 15, which is reminiscent of the trajectories found in section 2.3. For the same reasons as in section 3.2.3, one can also produce a variety of trajectories by varying the values of  $\omega_0$  and  $k$ , as shown in Figure 16.

We find that at least one stable periodic orbit exists in the  $(\psi_1, \psi_2)$  system between the saddle-node bifurcations of limit cycles at  $\mu_1 = \pm 0.115681$ . (For some parameters, there are two symmetry-related periodic orbits.) Within this range, there are several global bifurcations

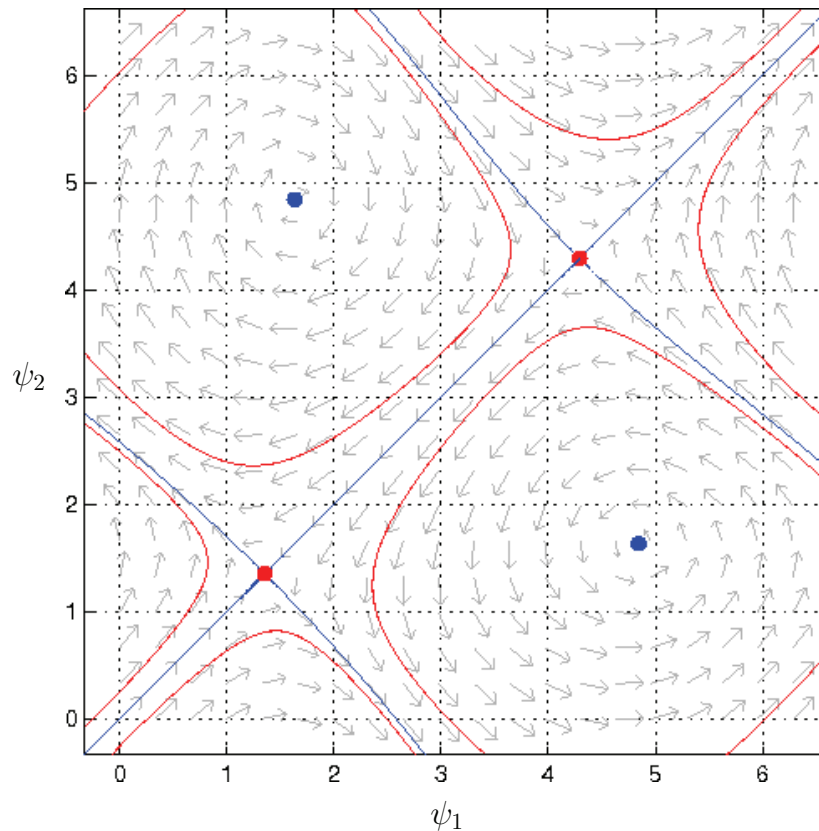


**Figure 14.** The  $(\psi_1, \psi_2)$  plane for the Arbiter coupling topology with  $N = 3$ , and coupling function (2.8) with  $\mu_1 = 0.1$ ,  $\mu_2 = 1$ ,  $\mu_3 = -0.06$ ,  $\omega_0 = 1$ ,  $k = 1$ . The existence of stable periodic orbits suggests that this system may provide interesting patterns of vehicular motion.

involving the  $S_2 \times S_1$  fixed points on the line  $\psi_1 = \psi_2$ . The details of these bifurcations are outside of the scope of our present study, but we do note that it would be possible to interpret the vehicular motion in terms of visits near and between the fixed points, as was done in section 3.

**5. Conclusion.** In this paper, we considered a model for vehicle motion coordination developed by Leonard, Paley, and Sepulchre which uses coupled oscillator steering control. We showed that novel trajectories are possible using only the phase controller when coupling functions more general than sinusoidal are considered. Such trajectories are associated with periodic orbits in the steering control subsystem, and the proximity of these periodic orbits to heteroclinic bifurcations allowed a detailed characterization of the properties of the vehicular trajectories.

Similar trajectories are expected to be possible for such systems with  $N > 3$  vehicles. An attempt to understand the details of such trajectories would likely benefit from previous studies of phase-locked solutions for coupled oscillator systems with phase-difference coupling [5, 6, 33] and heteroclinic orbits for such systems [3, 16].

The trajectories described in this paper may have applications in sensor area covering

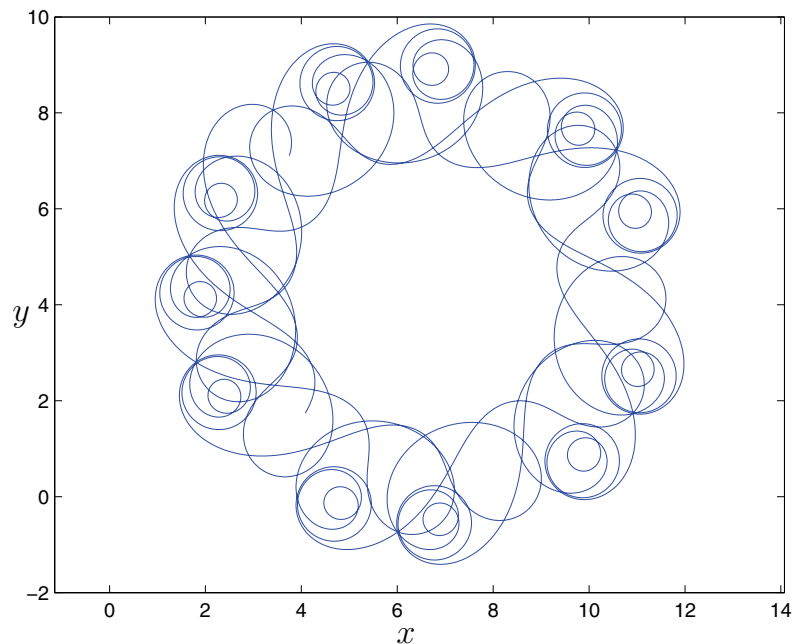


**Figure 15.** Motion of  $v_1$  using the Arbiter coupling topology with  $N = 3$  corresponding to the motion of the system along a stable periodic orbit in Figure 14.

problems in which one is particularly interested in certain regions of an annulus in the plane, with the option of either passing through the center or moving along the circumference of the area to be covered. For example, the trajectory shown in 1c of Figure 10 may be useful for the case where one wants agents to carefully patrol four evenly distributed areas as well as check the area in the center of those four areas periodically. If one desires to check sections of a circular area but is not interested in the area in the center of the sections, a trajectory such as 2e of Figure 11 may be appropriate. Should the areas inside the circular area be of higher interest than the perimeter, then a trajectory such as 2n of Figure 16 may be of interest. If one desires to patrol an annulus evenly in sections, a trajectory similar to 4e or 2f of Figure 11 may be useful. Most parameter values provide trajectories where an almost regular polygon-like global trajectory drifts around the center of pattern; thus, over time, the trajectories eventually cover an annulus. An example of this can be found in plot 3e of Figure 11—this is a “polygon” with slightly more than 2 sides, that is drifting around, and will eventually fill out an annulus. These patterns may be useful for applications where it is desirable for a robot patrolling an annulus-shaped space to not only periodically thoroughly investigate subregions of the space, but to also be relatively difficult to predict.

Despite the fact that the system is very stable in the reduced phase space, the trajectories described here are quite sensitive to variations in the parameters of the coupling equations. Should these trajectories prove to be potentially useful for a particular area coverage problem, it may be worthwhile to investigate the use of spacing control, and to make the global behavior robust to uncertainty and perturbations in the parameters.

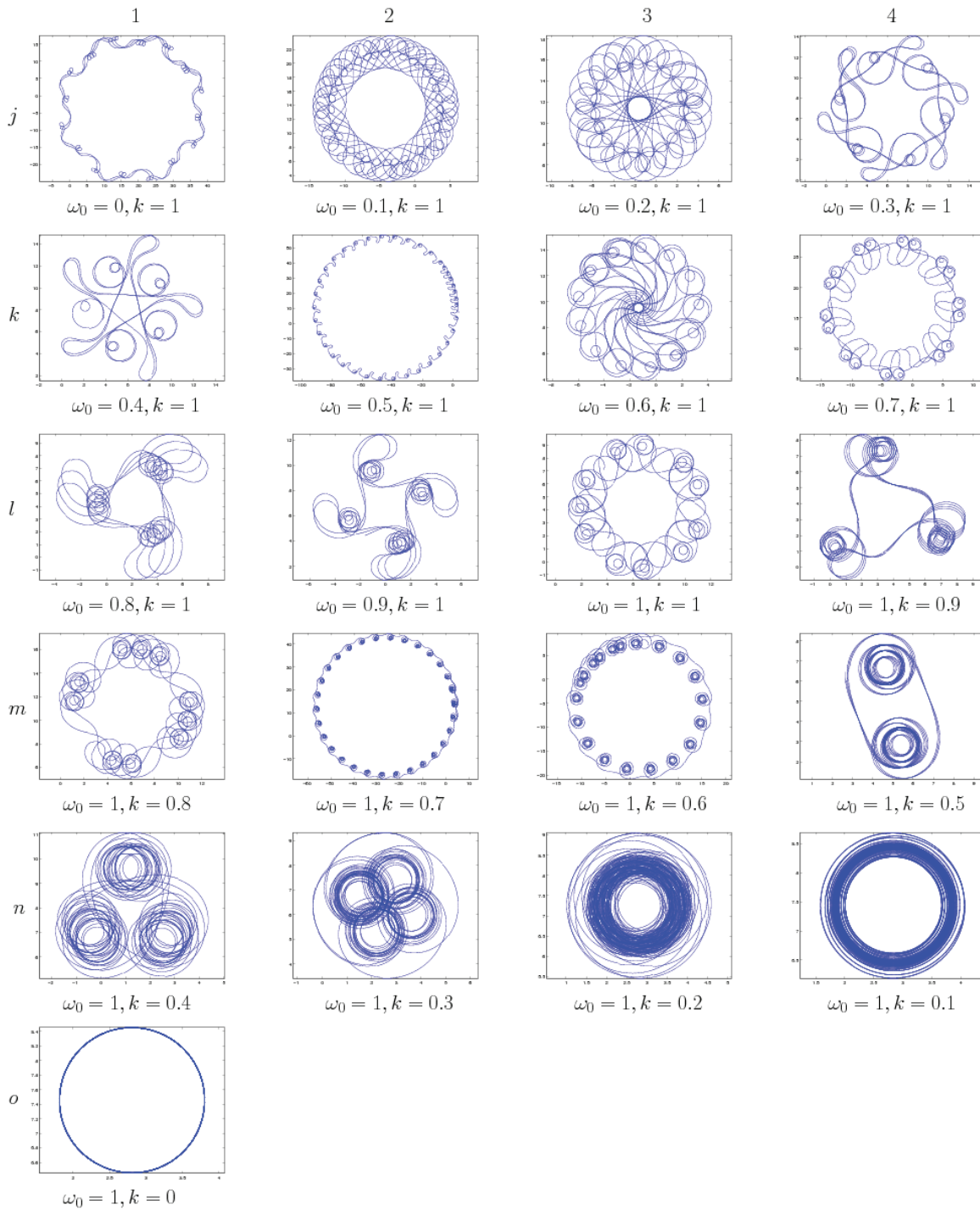


**Figure 16.** Various vehicular trajectories generated using the Arbiter coupling topology and the example coupling function (2.8) with  $\mu_1 = 0.1$ ,  $\mu_2 = 1$ ,  $\mu_3 = -0.06$ , while varying the values of  $\omega_0$  and  $k$ , as was done in Figures 10 and 11.

## REFERENCES

- [1] WIKIPEDIA, *Spirograph*, <http://en.wikipedia.org/wiki/Spirograph>.
- [2] P. ASHWIN, O. BURLKO, P. MAISTRENKO, AND O. POPVYCH, *Extreme sensitivity to detuning for globally coupled phase oscillators*, Phys. Rev. Lett., 96 (2006), 054102.
- [3] P. ASHWIN, O. BURLKO, AND Y. MAISTRENKO, *Bifurcation to heteroclinic cycles and sensitivity in three and four coupled phase oscillators*, Phys. D, 237 (2007), pp. 454–466.
- [4] P. ASHWIN, G. P. KING, AND J. W. SWIFT, *Three identical oscillators with symmetric coupling*, Nonlinearity, 3 (1990), pp. 585–601.
- [5] P. ASHWIN AND J. W. SWIFT, *The dynamics of  $n$  weakly coupled identical oscillators*, J. Nonlinear Sci., 2 (1992), pp. 69–108.
- [6] E. BROWN, P. HOLMES, AND J. MOEHLIS, *Globally coupled oscillator networks*, in Perspectives and Problems in Nonlinear Science: A Celebratory Volume in Honor of Larry Sirovich, E. Kaplan, J. Marsden, and K. R. Sreenivasan, eds., Springer-Verlag, New York, 2003, pp. 183–215.
- [7] S. CAMAZINE, J. L. DENEUBOURG, N. R. FRANKS, J. SNEYD, G. THERAULAZ, AND E. BONABEAU, *Self-Organization in Biological Systems*, Princeton University Press, Princeton, NJ, 2003.
- [8] L. CHAIMOWICZ, V. KUMAR, AND F. M. CAMPOS, *A paradigm for dynamic coordination of multiple robots*, Autonomous Robots, 17 (2004), pp. 7–21.
- [9] J. CORTÈS, S. MARTINES, T. KARATAS, AND F. BULLO, *Coverage control for mobile sensing networks*, IEEE Trans. Robot. Automat., 20 (2004), pp. 243–255.
- [10] J. P. DESAI, J. P. OSTROWSKI, AND V. KUMAR, *Modeling and control of formations of nonholonomic mobile robots*, IEEE Trans. Robot. Automat., 17 (2001), pp. 905–908.
- [11] L. E. DUBINS, *On curves of minimal length with a constraint on average curvature, and with prescribed initial and terminal positions and tangents*, Amer. J. Math., 79 (1957), pp. 497–516.
- [12] G. B. ERMENTROUT, *Simulating, Analyzing, and Animating Dynamical Systems: A Guide to XPPAUT for Researchers and Students*, Software Environ. Tools 14, SIAM, Philadelphia, 2002.
- [13] A. GARG, *Spirograph: Spirographs*, <http://wordsmith.org/~anu/java/spirograph.html>.
- [14] V. GAZI AND K. M. PASSINO, *Stability analysis of swarms*, IEEE Trans. Automat. Control, 48 (2002), pp. 692–696.
- [15] M. GOLUBITSKY, I. STEWART, AND D. G. SCHAEFFER, *Singularities and Groups in Bifurcation Theory, Vol. 2*, Springer-Verlag, New York, 1988.
- [16] D. E. HANSEL, G. MATO, AND C. MEUNIER, *Clustering and slow switching in globally coupled phase oscillators*, Phys. Rev. E (3), 48 (1993), pp. 3470–3477.
- [17] A. JADBABAIE, J. LIN, AND A. S. MORSE, *Coordination of groups of mobile autonomous agents using nearest neighbor rules*, IEEE Trans. Automat. Control, 48 (2003), pp. 692–696.
- [18] E. JUSTH AND P. KRISHNAPRASAD, *Equilibria and steering laws for planar formations*, Systems Control Lett., 52 (2004), pp. 25–38.
- [19] E. W. JUSTH AND P. S. KRISHNAPRASAD, *A Simple Control Law for UAV Formation Flying*, Technical report, Institute for Systems Research, University of Maryland, College Park, MD, 2002; available online from <http://www.lib.umd.edu/drum/handle/1903/6274?mode=simple>.
- [20] A. KOLPAS AND J. MOEHLIS, *Optimal switching between coexisting stable collective motion states*, Appl. Math. Lett., to appear.
- [21] N. LEONARD AND E. FIORELLI, *Virtual leaders, artificial potentials and coordinated control of groups*, in Proceedings of the 40th IEEE Conference on Decision and Control, IEEE Control Systems Society, Piscataway, NJ, 2001, pp. 2968–2973.
- [22] P. B. S. LISSAMAN AND C. A. SHOLLENBERGER, *Formation flight of birds*, Science, 168 (1970), pp. 1003–1005.
- [23] B. NABET, N. LEONARD, I. COUZIN, AND S. LEVIN, *Leadership in animal group motion: A bifurcation analysis*, in Proceedings of the 17th International Symposium on Mathematical Theory of Networks and Systems, Kyoto, Japan, 2006, pp. 1–14.
- [24] R. OLFATI-SABER, *Flocking for multi-agent dynamic systems: Algorithms and theory*, IEEE Trans. Automat. Control, 51 (2006), pp. 401–420.

- [25] D. PALEY, N. LEONARD, AND R. SEPULCHRE, *Collective motion: Bistability and trajectory tracking*, in Proceedings of the 43rd IEEE Conference on Decision and Control, IEEE Control Systems Society, Piscataway, NJ, 2004, pp. 1932–1937.
- [26] D. PALEY, N. LEONARD, AND R. SEPULCHRE, *Oscillator models and collective motion: Splay state stabilization of self-propelled particles*, in Proceedings of the 44th IEEE Conference on Decision and Control, IEEE Control Systems Society, Piscataway, NJ, 2005, pp. 3935–3940.
- [27] D. A. PALEY, N. E. LEONARD, R. SEPULCHRE, D. GRUNBAUM, AND J. PARRISH, *Oscillator models and collective motion*, IEEE Control Systems Magazine, 27 (2007), pp. 89–105.
- [28] B. L. PARTRIDGE, *The structure and function of fish schools*, Sci. Amer., 245 (1982), pp. 90–99.
- [29] R. SEPULCHRE, D. PALEY, AND N. LEONARD, *Collective motion and oscillator synchronization*, in Proceedings of the 2003 Block Island Workshop on Cooperative Control, V. Kumar, N. Leonard, and A. Morse, eds., Springer-Verlag, New York, 2003, pp. 1–17.
- [30] R. SEPULCHRE, D. PALEY, AND N. LEONARD, *Graph Laplacian and Lyapunov design of collective planar motions*, in Proceedings of the IEEE Conference on Nonlinear Theory and Its Applications, Bruges, Belgium, 2005, pp. 217–232.
- [31] R. SEPULCHRE, D. PALEY, AND N. LEONARD, *Stabilization of planar collective motion part I: All-to-all communication*, IEEE Trans. Automat. Control, 52 (2007), pp. 811–824.
- [32] A. R. E. SINCLAIR AND M. NORTON-GRIFFITHS, *Serengeti: Dynamics of an Ecosystem*, University of Chicago, Chicago, IL, 1979.
- [33] S. STROGATZ, *From Kuramoto to Crawford: Exploring the onset of synchronization in populations of coupled oscillators*, Phys. D, 143 (2000), pp. 1–20.
- [34] B. P. UVAROV, *Grasshoppers and Locusts*, Imperial Bureau of Entomology, London, 1928.